



Thermal and mechanical performance of electrospun chitosan/poly(vinyl alcohol) nanofibers with graphene oxide

Shuai Yang¹ · Yongxu Liu¹ · Zaixing Jiang² · Jiyu Gu¹ · Dawei Zhang¹ 

Received: 25 April 2018 / Accepted: 28 August 2018 / Published online: 21 September 2018
© Springer Nature Switzerland AG 2018

Abstract

In this paper, electrospun chitosan (CS)/poly(vinyl alcohol) (PVA)/graphene oxide (GO) nanofibers were fabricated. Prepared nanofibers have been characterized and investigated for their morphological, structural, and thermal stability, and mechanical and hydrophilic properties. The uniform and defect-free nanofibers were obtained and GO, shaping spindle and spherical, was partially embedded into nanofibers, as shown in SEM. The hydrogen bonds between CS molecules and PVA molecules were easily formed due to the great compatibility of CS and PVA. The addition of GO interrupted the hydrogen bonds between CS molecules and PVA molecules, and the new interaction was formed among CS, PVA, and GO. Thermogravimetric analysis indicated that as the increasing of content of GO, the thermal stability of nanofibers decreased. More interestingly, the static mechanical properties tests and dynamic mechanical analysis all showed that the modulus of nanofibrous mats increased firstly and decreased subsequently with the increasing of content of GO, which could be concerned with the looser arrangement of nanofibers. The water contact angle of nanofibrous mats increased with the increasing of content of GO. Nevertheless, when the content of GO was up to 2.5 wt%, the water contact angle decreased significantly.

Keywords Electrospun nanofibers · Chitosan · Graphene oxide · Thermal property · Mechanical performance

1 Introduction

Electrospun nanofibers have high surface area and highly porous structure. Besides, design flexibility and components controllability are great advantages of electrospun nanofibers. Because of the excellent properties resulted from these

structural advantages, electrospun nanofibers have the potential to be used widely in the range of protective textiles, filtration, composite reinforcement, and biomedical field such as tissue engineering scaffolds, wound dressings, and drug delivery [1]. Nevertheless, the great mechanical enhancement of electrospun fibers remains a fundamental challenge [2]. At present, there are various methods to improve the mechanical properties of nanofibrous mats, such as cross-linking, blending, and adding of reinforcing fillers [3]. The addition of nanofillers has been proved as an effective approach for achieving significant enhancement of the strength and fracture toughness of nanofibrous materials, showing combined advantages of the polymeric materials and fillers properties [4]. Over the past several years, natural and synthesis polymer nanocomposites with enhanced mechanical properties have been prepared successfully.

Chitosan (CS), derived from the chitin, is constituted of β -(1, 4)-linked glucosamino and N-acetyl glucosamino residues [5]. And it is one of the rare alkaline polysaccharides in nature with various physicochemical properties [6]. CS has been an attractive biopolymer for research in technology and biomedical fields, due to its abundance, low cost, and excellent biological properties. CS has been reported as an

✉ Zaixing Jiang
jiangzaixing@hit.edu.cn

✉ Dawei Zhang
zhangdawei@nefu.edu.cn

Shuai Yang
ys930509@163.com

Yongxu Liu
liuyongxu1995@163.com

Jiyu Gu
dldgujy@nefu.edu.cn

¹ College of Materials Science and Engineering, Northeast Forestry University, Harbin 150040, People's Republic of China

² School of Chemistry and Chemical Engineering, Harbin Institute of Technology, Harbin 150001, People's Republic of China

excellent candidate in filtration and ion absorption and as a biomaterial for enantioseparation, tissue engineering, drug delivery, and wound dressing [7]. Nevertheless, CS due to the existence of amino groups on the chains is not electrospinnable [8]. A common approach to improve the electrospinnability of CS is to blend it with other easily electrospinnable polymers such as poly(vinyl alcohol) (PVA), polyethylene oxide (PEO), and poly(lactic acid) (PLA) [9]. Due to the great compatibility between CS and PVA, PVA is commonly chosen to blend with CS for improving the electrospinnability, mechanical properties, and stability [10]. PVA has excellent biocompatibility, hydrophilic properties, and biomechanical characteristics [11] and it has been widely used in various biomedical applications such as wound dressing, tissue scaffold, and drug delivery [12].

The mechanical properties of CS nanofibers could be improved via the addition of reinforcing nanofillers [13]. Graphene oxide (GO) possesses amounts of oxygen-containing functional groups (such as epoxy, hydroxyl, carbonyl, and carboxyl functional groups [14]) on basal plates and edges, which could be cross-linked by polymers containing amino groups [15] for improving the mechanical stiffness and strength of composite materials [16]. It is worth noting that it is within the limits of reasonable concentration where GO is utilized for high strength nanofibers [17]. The integration and incorporation of GO into electrospun nanofibers will exert an influence on the physical and chemical properties. Meanwhile, the content of GO could be a significant element which determines the properties of nanofibers.

In this paper, electrospun CS/PVA nanofibers with different contents of GO have been fabricated and the effect of GO on morphology, chemical structure, crystallinity, thermal stability, and mechanical properties was investigated. Scanning electron microscopy (SEM) was used to characterize the morphology of nanofibers. The chemical structure, crystallinity, and thermal stability of nanofibers were measured using attenuated total reflection Fourier transform infrared spectroscopy (ATR-FTIR), X-ray diffraction (XRD), and thermogravimetric analysis (TGA). The static mechanical properties of nanofibrous mats were determined via a tensile strength tester and the dynamic mechanical properties were measured by dynamic mechanical analysis (DMA). Moreover, the hydrophilicity of nanofibrous mats was characterized by water contact angle test.

2 Experimental

2.1 Materials

CS (90–91%, deacetylation degree) was obtained from Zhejiang Golden-Shell Pharmaceutical Co., Ltd. PVA (degree of hydrolysis, 87–89%) was obtained from Aladdin Industrial,

Inc. Acetic acid was purchased from Tianjin Zhiyuan Reagent Co., Ltd. Natural graphite powder (5000 mesh) was commercially available from Qingdao Tianyuan Graphite Co., Ltd. H_2SO_4 (98 wt%) was purchased from Beijing Chemical Works. NaNO_3 was supplied by Tianjin Kermel Co., Ltd. KMnO_4 was purchased from Tianjin Chemical Reagent Factory and H_2O_2 (30 wt%) were obtained from Xilong Chemical Co., Ltd. Unless otherwise stated, all of the materials were of analytical grade and all of the materials were used as received without further treatment.

2.2 Preparation of GO dispersion

The GO was prepared using natural graphite as described elsewhere [18]. First, natural graphite powder was dried at 110 °C for 24 h. NaNO_3 was added and after, the graphite powder was cooled and placed in cold (0 °C) H_2SO_4 (98 wt%). Then KMnO_4 was gradually added with stirring, and the temperature of mixture was controlled in the range of 12–14 °C. The mixture was stirred for 4 h and an additional 30 min at 35 ± 3 °C. Distilled water was slowly added to mixture and the temperature was maintained in the range of 45–50 °C. Afterwards, the mixture was stirred at 90 °C for 30 min. The reaction was terminated by the addition of distilled water and H_2O_2 (30 wt%). The mixture was filtered and washed with distilled water for several times until the pH value of solution reached 6–7. Then the mixture was centrifuged at 5000 rpm for 5 min and the solid content of sediment was determined. GO dispersion (1 wt%), formed by adding appropriate amount of distilled water, was treated with ultrasonic to become uniform and homogeneous.

2.3 Preparation of CS/PVA/GO electrospun precursor solutions

CS powder was dissolved into distilled water with acetic acid (1% v/v) and stirred to obtain CS solution (2 wt%). PVA solution (5 wt%) was prepared by dissolving PVA powder into distilled water, then heated and stirred to obtain a homogeneous solution. The prepared CS solution, PVA solution, and GO dispersion were mixed according to the certain proportion. The solution mass ratio of CS and PVA was 1:3, and the content of GO was 0 wt%, 0.5 wt%, 1 wt%, 1.5 wt%, 2 wt%, and 2.5 wt%, respectively. The CS/PVA/GO electrospun precursor solutions were adequately stirred to obtain homogeneous mixing solutions.

2.4 Electrospinning process

The prepared electrospun precursor solution was filled in a 10 mL syringe connected to a flat-end metal needle with inner diameter of 0.9 mm. The applied voltage was 27 kV and the distance between needle tip and collector was 15 cm. The

needle, displayed with a horizontal plane of 15° , was perpendicular to the collecting plate. The electrospinning process was carried out by the pushing from gravity of electrospun precursor solution. The temperature was 25°C and relative humidity was less than 45%. After 20 h of electrospinning process, the prepared electrospun nanofibers were dried at 40°C for 24 h in a vacuum oven (-0.1 MPa). The schematic diagram of electrospinning process and structural representation of CS/PVA/GO nanofibers is shown in Fig. 1.

2.5 Morphology of prepared nanofibers

The morphology of prepared nanofibers was observed by field emission scanning electron microscopy (JSM-7500F, Jeol). Prior to the analysis, the samples were sputter-coated with gold for better conductivity during imaging. To determine the mean diameters and diameter distributions of prepared nanofibers, 80 different fibers were randomly selected, and the diameters were measured via Digimizer software.

2.6 Fourier transform infrared spectroscopy

The chemical structures of prepared nanofibers were investigated by attenuated total reflection Fourier transform infrared spectroscopy (Tensor II FTIR, Bruker). The spectral range was $4000\text{--}400\text{ cm}^{-1}$ with a resolution of 4 cm^{-1} .

2.7 X-ray diffraction analysis

XRD analysis was used to determine the crystallinity of prepared nanofibers. The XRD patterns were obtained on a XRD

analyzer (D/max-2200VPC, Rigaku) and a scanning rate was of $5^\circ/\text{min}$ over a 2θ range of $5^\circ\text{--}55^\circ$.

2.8 Thermogravimetric analysis

The thermal stability of prepared nanofibers was investigated using TGA (209 F3, Netzsch) under nitrogen atmosphere. The test temperature was at the range of $40\text{--}600^\circ\text{C}$ and heating rate was $10^\circ\text{C}/\text{min}$.

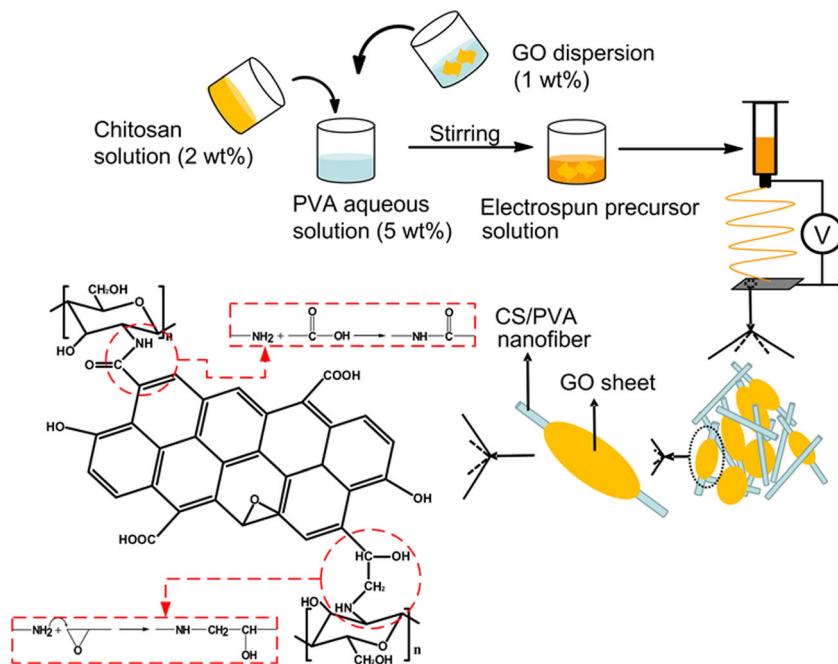
2.9 Mechanical properties

Mechanical properties of the nanofibrous mats were measured via a tensile strength tester (DSA 502A, Sans). The nanofibrous mats were cut into rectangle with sizes of $35 \times 10\text{ mm}$, and the sample gauge length was 20 mm. The thickness of each strip was measured. A tensile test was performed at a loading speed of $4\text{ mm}/\text{min}$ at 25°C and 45% relative humidity. Five samples were used to characterize each nanofibrous mat.

2.10 Dynamic mechanical analysis

Dynamic mechanical tests were performed on a dynamic mechanical analyzer (Q800, TA Instruments). The measurements were carried out in the tensile mode at constant frequency of 1 Hz and strain amplitude of 0.03%. The temperature was at the range of $40\text{--}150^\circ\text{C}$ using a heating rate of $5^\circ\text{C}/\text{min}$. Rectangular samples were cut from the nanofibrous mats at sizes of $5 \times 30\text{ mm}$ and the thickness of each sample was measured. The gap between jaws was 10 mm.

Fig. 1 The preparation process and structural representation of electrospun CS/PVA/GO nanofibers



2.11 Water contact angle

Static water contact angle (WCA) measurements of nanofibrous mats were recorded with a contact angle system (OCA 20, Dataphysics). The drop shape was recorded by a digital camera.

3 Results and discussion

3.1 Morphology of the prepared nanofibers

Figure 2 shows SEM images of electrospun CS/PVA nanofibers with different contents of GO and statistical representation of mean diameter of nanofibers (a), GO nanoparticles embedded in nanofibers (b). It could be observed that the homogeneous and uniform electrospun nanofibers without the occurrence of

bead defects were fabricated. As the increasing of content of GO, some bulges could be detected which were concerned with the GO sheets partially embedded into nanofibers, showing the shape of spindle and spherical. The mean diameter of nanofibers was determined by measuring 80 different fibers selected randomly via Digimizer software. The diameter distribution of nanofibers was in a narrow range of approximate 55 ± 7 nm. Moreover, there was a slight reduction in fiber diameter upon the addition of GO which could be ascribed by the modulation in electrospun solution parameters [19]. The addition of GO induced to the higher electrical conductivity and higher viscosity of electrospun precursor solutions [17], which provided eletrospinning solution higher tensile force when exposed to an applied voltage. As a result, the diameter of nanofibers became thinner. Meanwhile, as the increasing of content of GO, the diameter distribution of nanofibers became narrow, as illustrated in Fig. 2a. As the increasing of content of GO, the better distribution

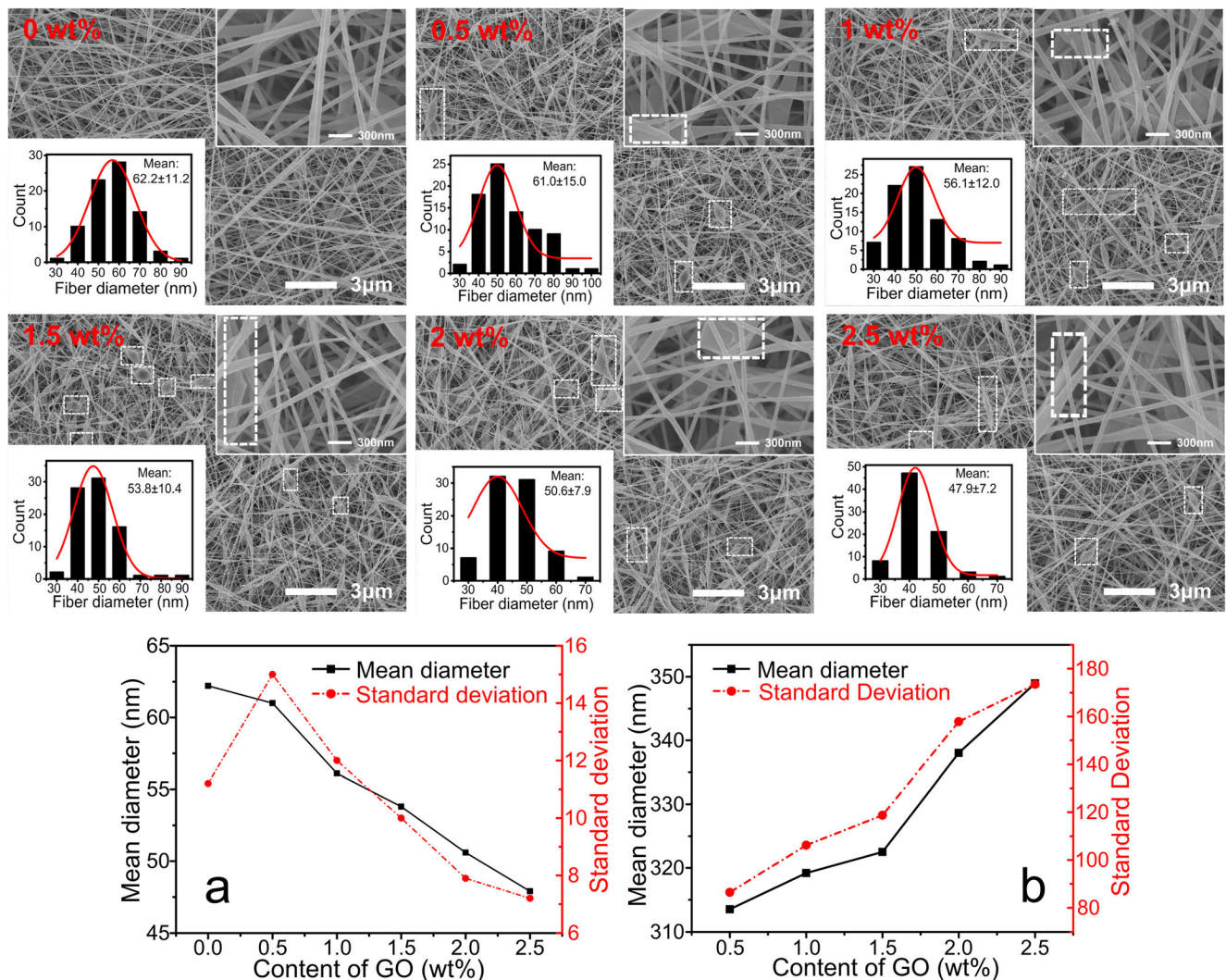


Fig. 2 SEM images and statistical representation show the effect of GO addition on the electrospun CS/PVA nanofibers morphology and diameter. The content of GO is 0 wt%, 0.5 wt%, 1 wt%, 1.5 wt%, 2 wt%, and

2.5 wt%. Statistical representation of mean diameter of nanofibers (a) and GO nanoparticles embedded in nanofibers (b)

of GO in nanofibers reduced the effect of inhomogeneous fibers arrangement on fibers diameter. In Fig. 2b, it could be observed that the diameter of GO nanoparticles embedded in nanofibers increased with the increasing of content of GO. It could be attributed to that the higher viscosity of electrospun precursor solutions, induced by the addition of GO, hindered the effect of self-constriction of GO nanosheets when the solvent volatilized during electrospinning process. Incompletely contracted GO nanoparticles shaped spindle and spherical, possessing larger sizes.

3.2 FTIR

FTIR spectra of CS powder, pure PVA nanofiber, electrospun CS/PVA nanofiber, and electrospun CS/PVA nanofiber with 2.5 wt% GO are shown in Fig. 3. The peak at 3640–2978 cm^{-1} could be attributed to the vibrational stretching of O-H [20] and N-H [21] bonds which became broad due to the existence of hydrogen bonds between CS and PVA. From the FTIR spectrum of CS, the peak at 2862 cm^{-1} was assigned to C-H stretching [22]. Feature peaks of amide I and amide II groups were observed at 1651 cm^{-1} and 1587 cm^{-1} [23], respectively. In the FTIR spectrum of PVA, the peak at 1725 cm^{-1} was concerned with C=O bond of residual ester groups, and the vibrational bending of C-H bond of PVA was observed at 1252 cm^{-1} [24]. The peak at 2918 cm^{-1} was assigned to C-H stretching, which shifted to a slightly lower wavenumber in CS. Comparing with the spectra of CS/PVA nanofiber with and without GO, there was no obvious difference between two curves. In fact, the epoxy groups on GO molecules could react with the amino groups on CS chains, which transformed primary -NH_2 groups into secondary -NH- groups. The peak of primary -NH_2 groups was so close to secondary -NH- groups that there were not obvious changes between two curves. Moreover, the carboxyl groups on GO sheets could react with the amino groups, and the peak of formed secondary -NH- groups was also not obvious in FTIR spectra [25]. In the dissolution test of prepared nanofibers, CS/PVA nanofiber was dissolved in the 90 °C acidic

aqueous solution (pH value 3–4), but CS/PVA nanofiber with 2.5 wt% GO was not. It could indicate that the cross-linking actions occurred between amino groups on CS chains and epoxy and carboxyl groups on GO sheets in nanofibers.

3.3 XRD

XRD patterns of CS powder, pure PVA nanofiber, and CS/PVA nanofibers with different contents of GO are performed in Fig. 4. In the curve of pure PVA nanofiber, there were two sharp diffraction peaks at $2\theta = 16.0^\circ$ and 22.4° , respectively. The pure CS showed the characteristic diffraction peak at $2\theta = 19.8^\circ$, which shifted slightly to 18.9° in CS/PVA nanofiber. As the increasing of content of GO, the peaks of CS/PVA nanofibers became broad, which indicated that the addition of GO decreased the crystallinity of CS/PVA nanofibers.

3.4 TGA

Figure 5 shows TGA curves of CS powder, pure PVA nanofiber, and electrospun CS/PVA nanofibers with different contents of GO. For CS powder, the TGA curve showed that at about 100 °C, the mass loss was about 2.9% which could be concerned with the loss of free water in CS molecules. A significant mass loss occurred at about 235 °C, indicating the beginning of degradation, which was concerned with the loss of amino and hydroxyl groups on CS chains. At about 355 °C, the mass loss was about 45.2% and the rate of degradation decreased due to the rigid and regular ring structure of CS chains. The residual mass of CS was about 43.5% when the temperature was up to 600 °C. The degradation of pure PVA nanofiber started at 247 °C and the mass loss was about 86.0% at 600 °C. In the curves of CS/PVA/GO nanofibers, the mass loss could be obtained at about 100 °C, which could be concerned with the free water and residual acid absorbed in nanofibers. There were two periods where the degradation rate was comparatively fast, at the range of 260–320 °C and 410–450 °C. At about 370 °C, the degradation rate decreased

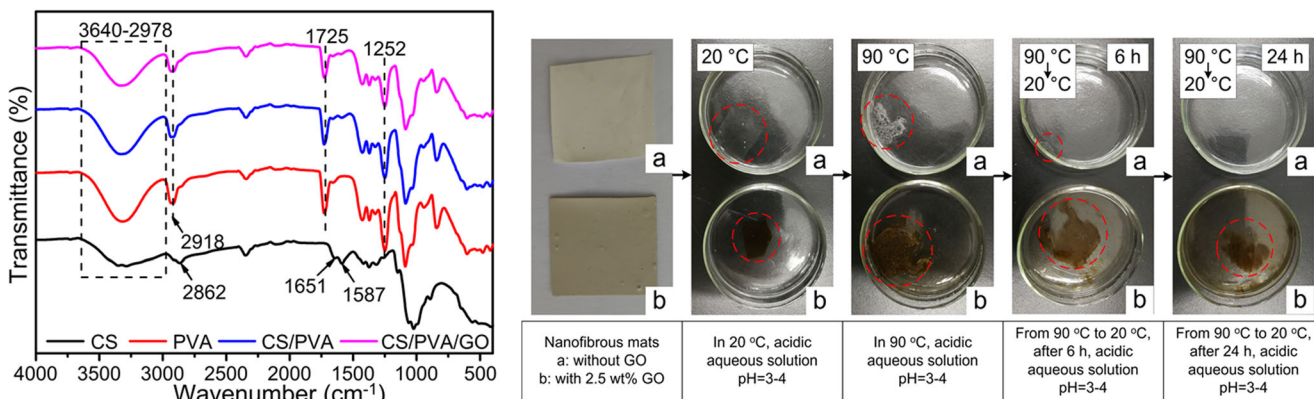


Fig. 3 FTIR spectra of the CS powder, pure PVA nanofiber, CS/PVA nanofiber, and CS/PVA nanofiber with 2.5 wt% GO and the dissolution test of prepared nanofibers, sample a: CS/PVA nanofiber; sample b: CS/PVA nanofiber with 2.5 wt% GO

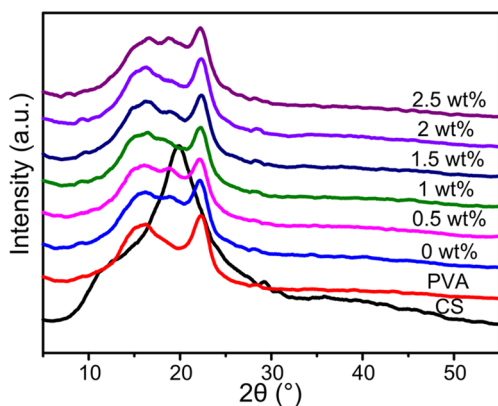


Fig. 4 XRD patterns of CS powder, pure PVA nanofiber, and electrospun CS/PVA nanofibers with different contents of GO (0 wt%, 0.5 wt%, 1 wt%, 1.5 wt%, 2 wt%, and 2.5 wt%)

significantly, shaping of smooth slope in the curves, which could be attributed to the occurrence of cross-linking reaction between amino groups on CS chains and epoxy and carboxyl groups on GO sheets during the heating and degradation process.

The temperatures of 5%, 10% degradation, and maximum degradation rate were chosen as the key temperature points to analyze the thermal stability of samples. Meanwhile, the mass fraction of samples at temperature of 600 °C was also recorded in Table 1. From Table 1, $T_{5\%}$, $T_{10\%}$, and T_{max} of CS/PVA/GO nanofibers increased firstly and then decreased. Indicatively, the addition of GO increased the degradation temperature. Nevertheless, when the content of GO increased constantly, the crystallinity of nanofibers decreased, and the degradation temperature decreased. Meanwhile, the good thermal conductivity of GO sheets accelerated the degradation of nanofibers [26]. The mass loss of nanofibers was up to 85% at 600 °C when the content of GO was 2.5%. As the increasing of content of GO, the mass loss increased which was concerned with the degradation of oxygen-containing functional groups on GO sheets [27].

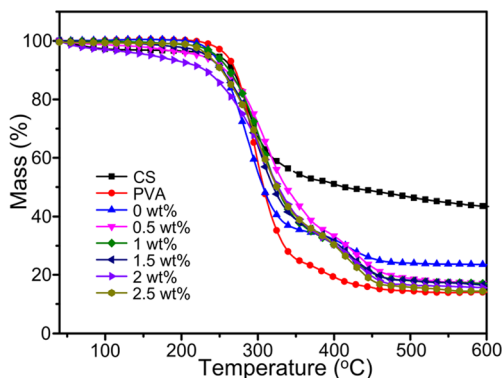


Fig. 5 TGA analysis of CS powder, pure PVA nanofiber, and electrospun CS/PVA nanofibers with different contents of GO (0 wt%, 0.5 wt%, 1 wt%, 1.5 wt%, 2 wt% and 2.5 wt%)

Table 1 Characteristic degradation temperatures and mass fraction for CS powder, pure PVA nanofiber, and electrospun CS/PVA nanofibers with different contents of GO (0 wt%, 0.5 wt%, 1 wt%, 1.5 wt%, 2 wt%, and 2.5 wt%). Obtained from TGA measurements in nitrogen atmosphere

Sample	$T_{5\%}$ (°C)	$T_{10\%}$ (°C)	T_{max} (°C)	ω_m (%)
CS	244.7	267.2	284.7	43.5
PVA	259.7	269.7	294.7	14.0
0 wt%	242.2	254.7	289.7	23.5
0.5 wt%	224.7	257.2	309.7	17.1
1 wt%	244.7	262.2	309.7	17.0
1.5 wt%	232.2	252.2	307.2	16.5
2 wt%	159.7	229.7	304.7	15.6
2.5 wt%	234.7	252.2	299.7	14.4

$T_{5\%}$ = initial degradation temperature obtained at 5% mass loss; $T_{10\%}$ = temperature corresponding to 10% mass loss; T_{max} = temperature of maximum degradation rate; ω_m = mass fractions at temperature of 600 °C

3.5 Mechanical properties of CS/PVA/GO nanofibrous mats

Tensile test results of electrospun CS/PVA nanofibrous mats with different contents of GO are shown in Fig. 6. In Fig. 6a, the tensile strength of nanofibrous mats decreased with the increasing of content of GO. As the increasing of content of GO, the arrangement of nanofibers became looser due to the increasing of the distance between fibers. During the electrospinning process, the disordered arrangement of fibers formed and the fibers overlapped with each other. Therefore, in the stretching process, stress could not pass on along the radial direction of nanofibers. The loose alignment of nanofibers hindered the continuous transmission of stress and the internal structure of nanofibrous mats was prone to be destroyed. The effect of stress concentration accelerated the fracture of nanofibrous mats. Besides, the loss in structural integrity of nanofibers with the higher content of GO might contribute to the phenomenon to some degree, because the nanofibers were “interrupted” along their length by large aggregates of GO. In Fig. 6b, the addition of GO significantly decreased the elongation at break of nanofibrous mats, which could be attributed to the effect of stress concentration caused by loose arrangement of nanofibers. The values of elongation at break of nanofibrous mats were so low that it could ascribe the fracture of nanofibrous mats as brittle fracture, as shown in Fig. 6c. In Fig. 6c, as the increasing of content of GO, Young’s modulus of nanofibrous mats increased firstly and decreased subsequently. The maximum occurred at 0.5 wt% GO, increased by 10.8 MPa due to the enhanced stiffness of nanofibrous mats. Nevertheless, the looser arrangement of nanofibers was harmful to the Young’s modulus and as a result, the Young’s modulus of nanofibrous mats decreased when the content of GO increased continually. Figure 6d

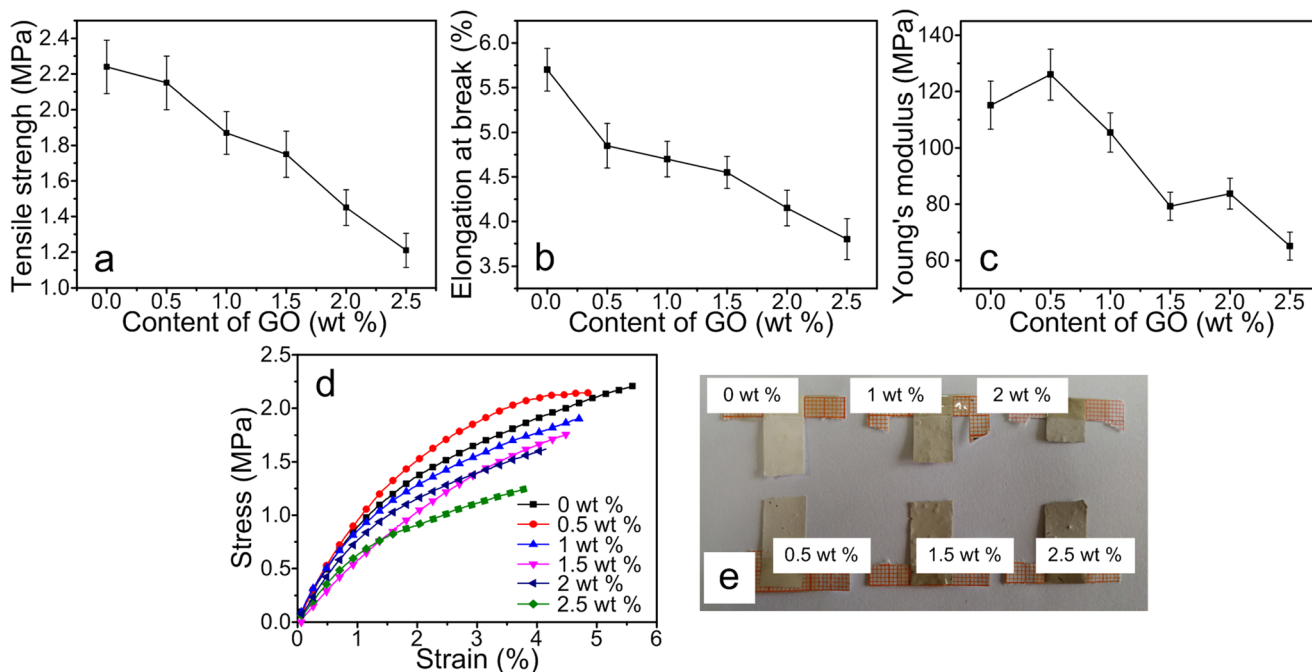


Fig. 6 Tensile test results of electrospun CS/PVA nanofibrous mats with different contents of GO (0 wt%, 0.5 wt%, 1 wt%, 1.5 wt%, 2 wt%, and 2.5 wt%): **a** tensile strength; **b** elongation at break, **c** Young's modulus, **d** typical stress-strain curves; **e** photo image of nanofibrous mats fracture

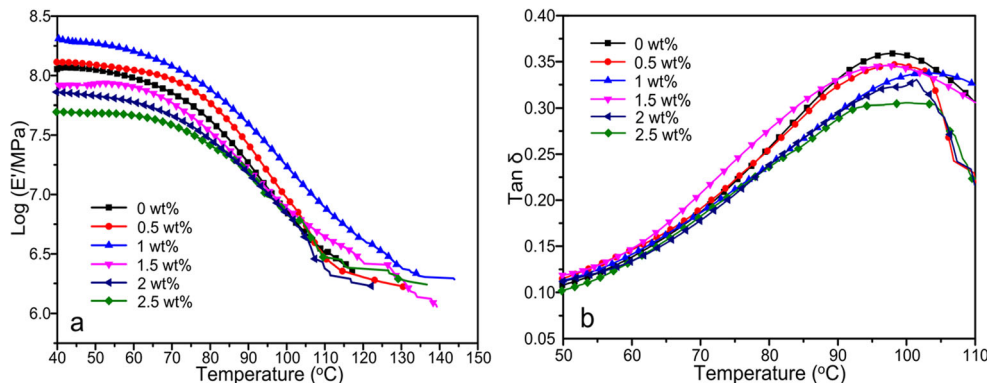
shows typical stress-strain curves of nanofibrous mats. It could be observed obviously that the fracture mode of nanofibrous mats was brittle fracture and Young's modulus increased firstly, decreased subsequently, as the increasing of content of GO.

3.6 DMA

In Fig. 7, the dynamic mechanical properties of electrospun CS/PVA nanofibrous mats with different contents of GO were measured by DMA. The curves of storage modulus as a function of temperature were plotted in (a) and $\tan \delta$ in (b). In Fig. 7a, the storage modulus of nanofibrous mats increased firstly, decreased subsequently with the increasing of content of GO. The maximum occurred at 1 wt% GO, increased by 75 MPa comparing with nanofibrous mat with 0 wt% GO. In

addition, the storage modulus of nanofibrous mats decreased with the higher content of GO, even to lower than which of nanofibrous mat with 0 wt% GO. It could be attributed to the looser arrangement of nanofibers with the increasing of content of GO. Figure 7b shows that the height of $\tan \delta$ of nanofibrous mats decreased constantly with the increasing of content of GO. It could be related to the addition of GO that enhanced the stiffness of nanofibers. Besides, the strong hindrance to chain mobility resulted from the strong interaction between functional groups on GO sheets, CS chains, and PVA molecules, which might contribute to the decreased $\tan \delta$ values. In addition, the epoxy and carboxyl groups on GO sheets could react with the amino groups on CS chains, engendering the cross-linking structures. Meanwhile, the increased cross-linking degree would also contribute to the glass transition temperature (T_g) of nanofibers shifted higher

Fig. 7 DMA analysis of CS/PVA nanofibrous mats with different contents of GO (0 wt%, 0.5 wt%, 1 wt%, 1.5 wt%, 2 wt%, and 2.5 wt%): **a** $\log E'$; **b** $\tan \delta$ curves



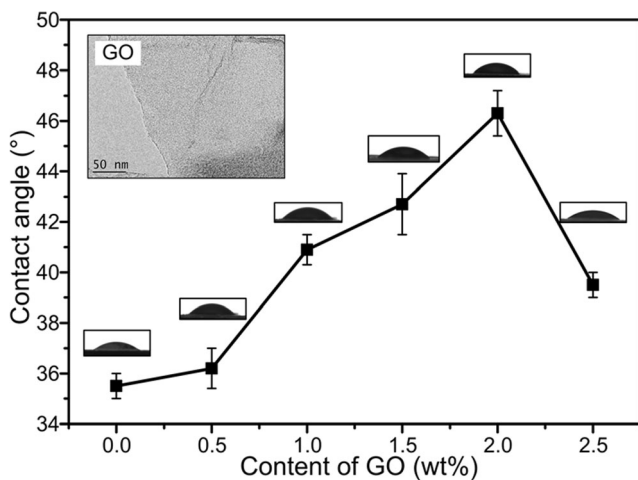


Fig. 8 Contact angle curves for electrospun CS/PVA nanofibrous mats with different contents of GO (0 wt%, 0.5 wt%, 1 wt%, 1.5 wt%, 2 wt%, and 2.5 wt%). Inset: water drop images for each mat surface

slightly (from 98.0 °C to 98.3 °C, 98.8 °C, and 99.5 °C, which corresponded to CS/PVA nanofibers with 0 wt%, 0.5 wt%, 2 wt%, and 2.5 wt% GO).

3.7 WCA

The hydrophilicity of electrospun CS/PVA nanofibrous mats with different contents of GO was estimated by water contact angle measurement, showed in Fig. 8. The water contact angle of 35.5° of nanofibrous mat with 0 wt% GO was observed and the contact angle slightly increased with the increasing of content of GO, from 36.2° to 40.9°, 42.7° and 46.3°, corresponding to the content of GO of 0.5, 1, 1.5, and 2 wt%, respectively. As the increasing of content of GO, the contact angle of nanofibrous mats increased due to the inhomogeneous of mat surface. Nevertheless, when the content of GO was up to 2.5 wt%, the contact angle decreased significantly, was 39.5°. When the content of GO increased continually, it would distribute homogeneous on mat surface. Besides, higher content of GO would increase the distance between fibers, conducive to the permeation of water, resulting in the decreased water contact angle.

4 Conclusion

CS/PVA nanofibers with different contents of GO were fabricated through electrospinning. The prepared nanofibers, possessed uniform, and smooth morphology, were obtained with a narrow diameter distribution of approximate 55 ± 7 nm. As the increasing of content of GO, the diameter distribution of nanofibers became narrow and the diameter of GO nanoparticles increased. The XRD patterns indicated that the addition of GO decreased the crystallinity of CS/PVA nanofibers. From TGA analysis, as the increasing of content of GO, the thermal

stability of nanofibers decreased. In the tensile test, the tensile strength and elongation at break of nanofibrous mats decreased with the increasing of content of GO. Nevertheless, the Young's modulus increased firstly and decreased subsequently, and the maximum occurred at 0.5 wt% GO. In DMA curves, the storage modulus of nanofibrous mats increased firstly and decreased subsequently, and the maximum occurred at 1 wt% GO. Meanwhile, with the increasing of GO, the $\tan \delta$ values decreased and the T_g shifted slightly higher. In water contact angle tests, as the increasing of content of GO, the water contact angle of nanofibrous mats increased. When the content of GO was up to 2.5%, the contact angle decreased significantly to 39.5°. These properties would provide electrospun CS/PVA/GO nanofibers potential applications in biomedical fields wanted mechanical performance such as wound dressing, tissue engineering, and artificial scaffold.

Funding information This research was financially supported through grants from the Fundamental Research Funds for the Central Universities (2572018BB10) and Heilongjiang Postdoctoral Foundation Assistance (LBH-Z13010), National Program for Support of Top-notch Young Professionals, National Natural Science Foundation of China (51773049), China Aerospace Science and Technology Corporation-Harbin Institute of Technology Joint Center for Technology Innovation Fund (HIT15-1A01), Harbin city science and technology projects (2013DB4BP031 and RC2014QN017035), China Postdoctoral Science Special Foundation (201003420 and 20090460067), HIT Research Institute (Zhao Yuan) of New Materials and Intelligent Equipment Technology Co., Ltd., and Scientific and Technological Cooperation and Development Fund (2017KJHZ002).

Compliance with ethical standards

Conflict of interest The authors declare that they have no conflict of interest.

References

1. Maleki H, Gharehaghaji AA, Dijkstra PJ (2017) Electrospinning of continuous poly (L-lactide) yarns: effect of twist on the morphology, thermal properties and mechanical behavior. *J Mech Behav Biomed Mater* 71:231–237
2. Guo FY, Wang N, Hou LL, Liu JC, Wang L, Zhao Y (2017) Mechanical enhancement of bi-phasic electrospun nanofibrous films by optimizing composition and configuration. *Mater Chem Phys* 193:220–226
3. Corsello FA, Bolla PA, Anbinder PS, Serradell MA, Amalvy JI, Peruzzo PJ (2017) Morphology and properties of neutralized chitosan-cellulose nanocrystals biocomposite films. *Carbohydr Polym* 156:452–459
4. Karimi B, Ramezanzadeh B (2017) A comparative study on the effects of ultrathin luminescent graphene oxide quantum dot (GOQD) and graphene oxide (GO) nanosheets on the interfacial interactions and mechanical properties of an epoxy composite. *J Colloid Interface Sci* 493:62–76
5. Zhang CP, Zhang Y, Hao XY, Liu H, Lv X, Zhu JF, Han WL, Zhang YH (2018) Fabrication of reduced graphene oxide/chitosan composite fiber by dry-jet wet spinning. *Adv Compos Hybrid Mater*. <https://doi.org/10.1007/s42114-018-0029-2>

6. Zhang DW, Yang S, Chen YQ, Liu SY, Zhao HT, Gu JY (2018) ^{60}Co -ray irradiation crosslinking of chitosan/graphene oxide composite film: swelling, thermal stability, mechanical, and antibacterial properties. *Polymers* 10:294
7. Lancina MG, Shankar RK, Yang H (2017) Chitosan nanofibers for transbuccal insulin delivery. *J Biomed Mater Res A* 105(5):1252–1259
8. Elsabee MZ, Naguib HF, Morsi RE (2012) Chitosan based nanofibers, review. *Mat Sci Eng C* 32(7):1711–1726
9. Nguyen TTT, Tae B, Park JS (2011) Synthesis and characterization of nanofiber webs of chitosan/poly(vinyl alcohol) blends incorporated with silver nanoparticles. *J Mater Sci* 46:6528–6537
10. Wang Q, Fu YJ, Yan XX, Chang YJ, Ren LL, Zhou J (2017) Preparation and characterization of underwater superoleophobic chitosan/poly(vinyl alcohol) coatings for self-cleaning and oil/water separation. *Appl Surf Sci* 412:10–18
11. Choi J, Panthi G, Liu Y, Kim J, Chae SH, Lee C, Park M, Kim HY (2015) Keratin/poly(vinyl alcohol) blended nanofibers with high optical transmittance. *Polymer* 58:146–152
12. Ghasemi HH, Rezvani Z, Nazm BM, Shirinzadeh H, Seifalian AM, Joghataei MT, Razaghpour M, Alibakhshi A, Yazdanpanah A, Salimi M, Mozafari M, Urbanska AM, Reis RL, Kundu SC, Gholipourmalekabadi M (2017) Chitosan-intercalated montmorillonite/poly(vinyl alcohol) nanofibers as a platform to guide neuron-like differentiation of human dental pulp stem cells. *ACS Appl Mater Interfaces* 9(13):11392–11404
13. Cai N, Hou DJ, Luo XG, Han C, Fu J, Zeng H, Yu FQ (2016) Enhancing mechanical properties of polyelectrolyte complex nanofibers with graphene oxide nanofillers pretreated by polycation. *Compos Sci Technol* 135:128–136
14. Wang ZY, Yan S, Sun YJ, Xiong T, Dong F, Zhang W (2017) Glassy carbon electrode modified with 7, 7, 8, 8-tetracyanoquinodimethane and graphene oxide triggered a synergistic effect: low-potential amperometric detection of reduced glutathione. *Appl Catal B Environ* 214:148–157
15. Hung WS, Tsou CH, De Guzman M, An QF, Liu YL, Zhang YM, Hu CC, Lee KR, Lai JY (2014) Cross-linking with diamino monomers to prepare composite graphene oxide-framework mats with varying d-spacing. *Chem Mater* 26(9):2983–2990
16. Yavuz E, Tokalioglu S, Sahan H, Kacer M, Patat S (2017) Dispersive solid-phase extraction of rhodium from water, street dust, and catalytic converters using a cellulose-graphite oxide composite. *Anal Lett* 50(1):63–79
17. Liu Y, Park M, Shin HK, Pant B, Choi J, Park YW, Lee JY, Park SJ, Kim HY (2014) Facile preparation and characterization of poly(vinyl alcohol)/chitosan/graphene oxide biocomposite nanofibers. *J Ind Eng Chem* 20(6):4415–4420
18. Marcano DC, Kosynkin DV, Berlin JM, Sinitskii A, Sun Z, Slesarev A, Alemany LB, Lu W, Tour JM (2010) Improved synthesis of graphene oxide. *ACS Nano* 4(8):4806–4814
19. Mahmoudi N, Simchi A (2017) On the biological performance of graphene oxide-modified chitosan/polyvinyl pyrrolidone nanocomposite mats: in vitro and in vivo effects of graphene oxide. *Mat Sci Eng C Mater Biol Appl* 70:121–131
20. Cheng F, Gao J, Wang L, Hu XY (2015) Composite chitosan/poly(ethylene oxide) electrospun nanofibrous mats as novel wound dressing matrixes for the controlled release of drugs. *J Appl Polym Sci* 132(24):42060
21. Usman A, Hussain Z, Riaz A, Khan AN (2016) Enhanced mechanical, thermal and antimicrobial properties of poly(vinyl alcohol)/graphene oxide/starch/silver nanocomposites films. *Carbohydr Polym* 153:592–599
22. Kohsari I, Shariatnia Z, Pourmortazavi SM (2016) Antibacterial electrospun chitosan-polyethylene oxide nanocomposite mats containing bioactive silver nanoparticles. *Carbohydr Polym* 140:287–298
23. Poornima B, Korrapati PS (2016) Fabrication of chitosan-polycaprolactone composite nanofibrous scaffold for simultaneous delivery of ferulic acid and resveratrol. *Carbohydr Polym* 157:1741–1749
24. Habiba U, Siddique TA, Joo TC, Salleh A, Ang BC, Afifi AM (2017) Synthesis of chitosan/polyvinyl alcohol/zeolite composite for removal of methyl orange, congo red and chromium(VI) by flocculation/adsorption. *Carbohydr Polym* 157:1568–1579
25. Ma LB, Zhang Y, Wang SQ (2016) Modified treatment for carbonized cellulose nanofiber application in composites. *Compos A Appl Sci Manuf* 90:786–793
26. Gorji M, Karimi M, Larki MR, Safavi A (2017) Theoretical modeling of thermal stress imposed by selective permeation mats reinforced with graphene oxide. *J Appl Polym Sci* 134(17):44752
27. Dubey P, Gopinath P (2016) PEGylated graphene oxide based nanocomposite grafted chitosan/polyvinyl alcohol nanofiber as an advanced antibacterial wound dressing. *RSC Adv* 6(73):69103–69116